ACS APPLIED MATERIALS & INTERFACES

Research Article

www.acsami.org

Faujasites Incorporated Tissue Engineering Scaffolds for Wound Healing: In Vitro and In Vivo Analysis

Neethu Ninan,*[,†,‡] Muthunarayanan Muthiah,[§] In-Kyu Park,[§] Anne Elain,[†] Tin Wui Wong,[⊥] Sabu Thomas,[‡] and Yves Grohens[†]

[†]Laboratoire Ingénierie des Matériaux de Bretagne, Université de Bretagne Sud, BP 92116, 56321 Lorient Cedex, France

[‡]Centre for Nanoscience and Nanotechnology and School of Chemical Sciences, Mahatma Gandhi University, Priyadarsini Hills PO, Kottayam 686 560, Kerala, India

[§]Department of Biomedical Sciences, Chonnam National University Medical School, Gwangju 501-757, South Korea

[⊥]Non-Destructive Biomedical and Pharmaceutical Research Centre, Universiti Teknologi MARA, 42300 Puncak Alam, Selangor, Malaysia

Supporting Information

ABSTRACT: Exploring the possibility of using inorganic faujasites in tissue engineering scaffolds is a prospective approach in regenerative medicine. Novel gelatin/hyaluronic acid (HA)/faujasite porous scaffolds with low surface energy were fabricated by lyophilization. The pore size of gelatin/HA scaffold was 50−2000 μm, whereas it was greatly reduced to 10−250 μm after incorporation of 2.4% (w/w) of faujasites in polymer matrix, GH(2.4%). Micro computed tomography analysis showed that the porosity of GH(2.4%) was 90.6%. The summative effect was ideal for growth of dermal fibroblasts and cellular attachment. XRD analysis revealed that the embedded faujasites maintained their crystallinity in the polymer matrix even though they interacted with the polymers as indicated by FT-IR analysis. Coupling with effective reinforcement of faujasites, GH(2.4%) demonstrated compression modulus of 929 ± 7 Pa and glass transition temperature of 31 ± 0.05 °C. It exhibited controlled swelling and degradation, allowing sufficient space for tissue regrowth. The latter is further supported by capability of faujasites to provide efficient oxygen supply to fibroblast cells. GH(2.4%) showed a cell viability of 91 ± 8% on NIH 3T3 fibroblast cell lines. The in vivo studies on Sprague−Dawley rats revealed its ability to enhance wound healing by accelerating re-epithelization and collagen deposition. These findings indicated its potential as excellent wound dressing material.

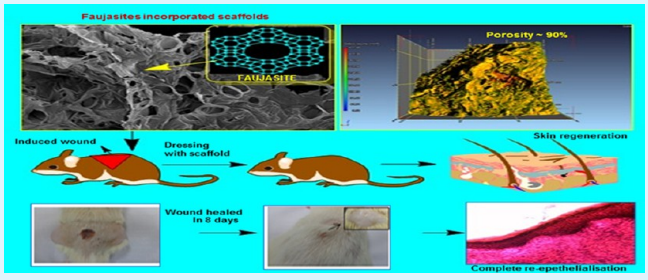

KEYWORDS: *gelatin, hyaluronic acid, faujasite, composite, wound healing, fibroblast*

INTRODUCTION

Wound healing is a multifaceted regenerative process involving four phases, namely, hemostasis, inflammation, proliferation, and remodelling.[1] When skin is injured, the damaged blood vessels are immediately sealed by platelets. Hemostasis is initiated by clotting factors that results in the formation of fibrin network, producing a clot in the wound, causing bleeding to stop.[2] Inflammation befalls simultaneously with hemostasis in which vasodilation occurs through release of chemicals like histamine and serotonin.[3] The microorganisms and debris are engulfed by neutrophils and macrophages. During the proliferative phase, granulation tissue is formed along with fibroblast infiltration and collagen synthesis.[4] The remodelling phase involves the formation of cellular connective tissue and strengthening of epithelium.[5] Wound infection can severely prolong the healing process. If left untreated, the infection may spread to other parts of the body and can prove to be life threatening.[6] The characteristics of an ideal wound dressing material are to maintain moist environment, absorb excess exudates, allow gas exchange, and protect from microbial infection.[7]

Several biopolymers are used for synthesizing wound dressing materials like chitin,[8] chitosan,[9] alginate,[10] silk fibroin,[11] gelatin,[12] collagen,[13] hyaluronic acid,[14] chondroitin sulfate,[15] carboxymethylcellulose,[16] poly lactic acid,[17] poly lactic-co-glycolic acid,[18] polyurethane,[19] dextran,[20] etc. Gelatin is a protein formed by partial hydrolysis of collagen, consisting of positively and negatively charged amino acids along with hydrophobic domains, folded into a stable super helical structure.[21] It is nonimmunogenic, biocompatible, and biodegradable.[22] It has been widely used in drug delivery,[23] tissue engineering,[24] and coating tissue culture dishes.[25] Hyaluronic acid (HA) is an anionic biopolymer that is nonimmunogenic, nonadhesive and nonthrombogenic.[26] It is composed of N-

Received: August 16, 2013
Accepted: October 8, 2013
Published: October 8, 2013

acetyl-D-glucosamine and D-guluronic acid and is highly viscoelastic. It is a major component of extracellular matrix (ECM) and is vital for cell−receptor interactions, cellular proliferation, angiogenesis, and wound healing.[27] Both gelatin and HA, when used individually face some challenges. The main drawback of gelatin is poor mechanical performance and the limitation of HA is its nonadhesive nature.[28] So, HA is incorporated within gelatin matrix to mimic ECM of skin with improved mechanical integrity and provide a suitable microenvironment for cell growth imparting sufficient cell adhesiveness. Wang et al., has used a polyblend of gelatin−hyaluronic acid−chondroitin sulfate scaffolds for wound healing, but it would have been beneficial if these scaffolds contain moieties that meet oxygen demands of the dermal fibroblasts.[29]

Zeolites are solid inorganic aluminosilicates with uniform microporous architecture. The net negative charge of zeolite is compensated by extra framework cations and thus they exhibit cation exchange ability.[30] They are used as MRI contrast agents,[31] antibacterial agents,[32] and drug carriers for anticancer molecules,[33] and for tissue engineering.[34] Morsli et al., has synthesized zeolite/chitosan composites and verified that they are ideal for catalysis and separation.[35] Recently, Yu et al. has confirmed the antimicrobial activity of chitosan/zeolite-A hybrid composites for tissue engineering.[36] Seifu et al., has proved that fluorinated zeolites are capable of providing sufficient oxygen supply to cells.[34] Among the different zeolites, faujasites play a vital role in biomedical applications as their pores are small enough to entrap drug or biological molecules.[37] Their frameworks consist of eight sodalite cages which are linked together forming a large central cavity or supercage with a diameter of 12 Å. The supercages possess a 12 membered ring with a diameter of 7 Å.[38] Because of their large surface area, they can be easily adsorbed onto polymers and are used as filler materials to enhance mechanical and thermal performance of biocomposites.[39]

We have made an attempt to explore whether faujasites incorporated within gelatin/HA matrix can increase oxygen supply to cells and thereby promote wound healing. The morphological, mechanical, thermal and biological properties of the lyophilized scaffolds were investigated in detail. The in vivo studies on Sprague−Dawley rats were conducted to prove whether the prepared scaffolds enhanced wound healing and promoted faster re-epithelization and collagen deposition.

MATERIALS AND METHODS

Materials. HA was purchased from Acros Organics (Geel, Belgium). Gelatin (type B) was procured from Merck Chemicals (Damstadt, Germany). Glycerol (purity~99%) and formaldehyde (36.5−38%) were obtained from Sigma Aldrich (Saint Quentin Fallavier, France). Z_F was a kind gift from IRMA (Ploemeur, France). Phosphate buffered saline (PBS), endotoxin free water, Dulbecco's Modified Eagle's Medium (DMEM), absolute ethanol and MTS reagents were bought from Sigma Aldrich. Hydrochloric acid, ammonia, diethyl ether and xylene were obtained from Merck chemicals (Damstadt, Germany). The staining reagents like Harris hematoxylin and eosin were acquired from Leica Biosystems Richmund Inc. (Germany). Ketamine hydrochloride and xylazine hydrochloride were bought from Troy laboratories, Australia. All the reagents used in the synthesis were of analytical grade and were not further purified. NIH 3T3 fibroblast cells were acquired from ATCC cell biology collection. Male Sprague−Dawley rats were collected from Genetic Improvement and Farm Technologies Sdn Bhd Malaysia.

Fabrication of Lyophilized HA/Gelatin/Z_F Scaffold. A 0.5% (w/v) HA solution was prepared by dissolving 1.0g HA in water, kept in ice bath. The water used for synthesis was devoid of endotoxin. A 2% (w/v) of gelatin solution was formulated by dissolving 2g of gelatin powder in water by magnetic stirring at 60 °C. HA was added to gelatin solution by syringe addition and stirred vigorously for 1 h. To this, 5% (v/v) of glycerol was added as a plasticizer and further stirred. Then, 2.40% (w/w) of Z_F was dispersed in water, and sonicated for 30 min. The activated zeolite suspension was added to HA/gelatin solution. After complete intermixing of polymer and inorganic filler, the solution was cross-linked by 0.38% (v/v) of formaldehyde. The resulting viscous sample was then transferred to petriplates and prefrozen at −20 °C in a deep freezer. The frozen samples were lyophilized in Christ Alpha 1−2 LD Plus freeze-dryer to fabricate porous HA/gelatin/Z_F scaffold. By keeping all other parameters constant, composites scaffolds were prepared with 0.24, 0.48, 2.40, and 4.80% (w/w) of Z_F, namely, GH(0.24%),GH(0.48%), GH(2.4%), and GH(4.8%), respectively. GH(0%) was the control scaffold prepared without any Z_F.

Physicochemical Characterization. The surface morphology of the prepared scaffolds was inspected using Scanning electron microscope (SEM) (JEOL, JSM 6031 from Kyoto, Japan). Thin sections of the samples were excised using razor blade, sputter coated with gold using Polaron Sputtering apparatus and examined. Triplicates of samples were analyzed and pore size distribution profile was plotted using ImageJ software. The material compositions of the prepared scaffolds and Z_F were estimated from by Energy dispersive X-ray spectroscopy (EDX) (Oxford INCA Energy 200 Premium, Japan). The dispersion of the Z_F particles in the scaffold matrix was studied from silicon mapping.

Micro computed tomography (Micro-CT) was conducted at Morlaix, France using monochromatic beam of X-rays with energy of 240 kV/320W. A series of two-dimensional (2D) images were acquired by rotating sample of thickness 2.5 mm along 360° angle. These 2D images were then reconstructed to form 3D images, through several steps like recording of projection, logarithm, ramp filtering and back projection. The maximum object diameter was 50 cm and the distance between sample and detector was 1500 mm. The acquisition speed was 15 frames/s and the length of precision manipulator was 60 cm. Triplicates of samples were analyzed and pore size distribution profile was plotted. The porosity of the scaffold was determined by defect analysis, using following equation.

$$\text{porosity} = [V_1/(V_1 + V_2)]$$

where V_1 is the defect volume and V_2 is the volume of scaffold.

Contact angle measurements were performed with contact angle meter (GBX Digidrop, France) equipped with a high resolution 2/3 in. CCD camera. The scaffolds were cut into rectangular sections ($5 \times 2 \times 1$ cm^3) and kept flat on a plane solid support, maintained at 25 °C. Drop orientation was determined using sessile drop method. The liquid droplet volume was 6.0 ± 0.5 μL and images of droplets were seized after every 30s, using a camera. The liquid was dropped on different corners of each sample and average of contact angle was tabulated. Water, formamide and tricresyl phosphate were the polar and apolar liquids used to evaluate surface energy. Owens and Wendt equation was used to estimate surface energy.[40] Replicates of samples were done and the averages of these values were tabulated.

The potential interaction between polymers and inorganic filler was evaluated using Fourier transform infrared (FTIR) spectrometer (Shimadzu 8400M, Japan), by spanning along a frequency range from 400 to 4000 cm^{-1}. To comprehend the physical nature of Z_F in the composite scaffold, X-ray diffraction analysis (XRD), was done using diffractometer (Philips PW3710, France) operating at 40KV and 40 mA with CuKα radiation at a wavelength of 1.5418 Å. The diffraction spectrum was recorded, analyzed and phase matched by X'PERT software and graphics. The variation in glass transition temperature (T_g) in case of composite scaffolds was measured by differential scanning calorimetry (DSC) analysis (Mettler-Toledo DSC-882, France). Ten milligram samples were weighed in aluminum pans and heated at 5 °C/min, with constant purging of nitrogen at 50 mL/min, over a temperature range from 10 to 80 °C.

A dynamic mechanic analyzer (DMA 2980 TA, France) was used to analyze the mechanical properties of the prepared scaffolds. Compression testing was done on rectangular specimens ($2 \times 2 \times 0.6$

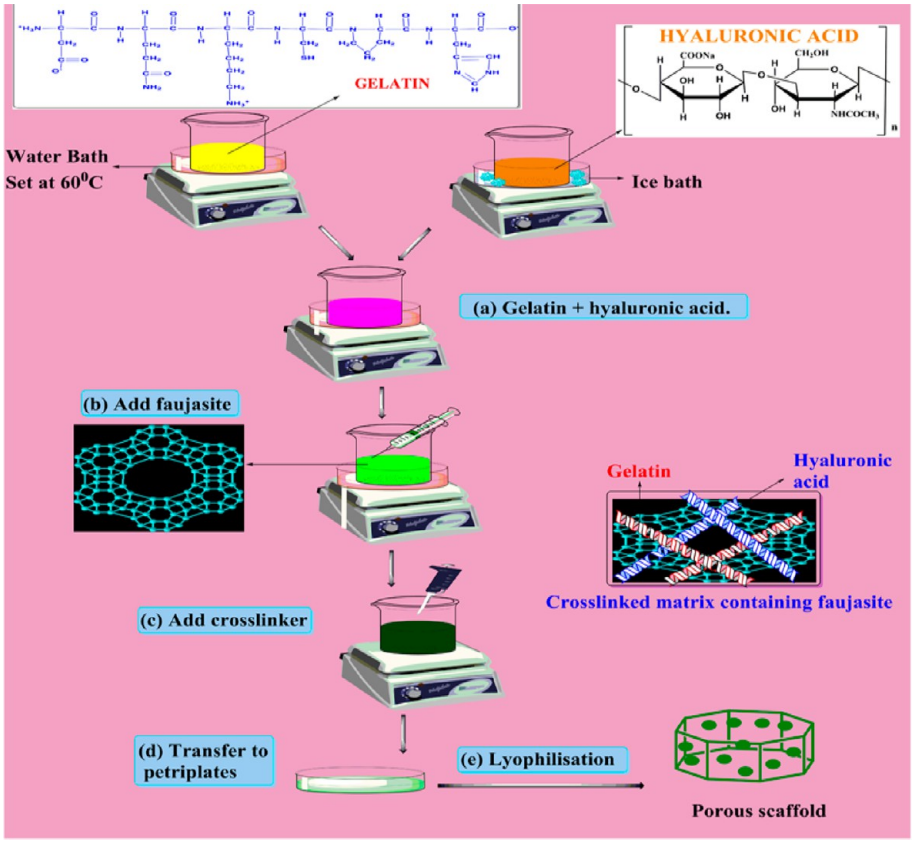

Figure 1. Schematic diagram showing the synthesis of Gelatin/HA/Z_F hybrid scaffold by (a) mixing gelatin and HA, (b) adding Z_F to the mixture, (c cross-linking the mixture, (d) transferring the mixture to petriplates, followed by (e) lyophilization.

cm^3) by subjecting them to a static load that increased at the rate of 100 mN/min. The compression modulus was obtained from the slope of the linear region of stress−strain curve. Six samples of each composition were tested and their average was recorded.

Water Uptake Studies. The water uptake ability of the scaffolds was analyzed for 14 days. An ideal scaffold should be able to absorb and retain excess moisture at wound site without undergoing uncontrolled swelling. The samples were cut into small pieces of equal weights and immersed in deionized water at 37 °C. The soaked samples were removed after required period of time, blotted on filter paper till no more water was left and weighed. The initial and final weights were noted as W_1 and W_2 and percentage of water uptake was determined by subsequent equation. Triplicates of samples were done and the average was plotted.

$$\text{percentage of water uptake}(\%) = 100 \times (W_2 - W_1)/W_1$$

In Vitro Degradation Studies. The biodegradation of scaffolds was investigated by immersing accurately weighed scaffolds of equal size in PBS (pH ~7.4) at 37 °C, for 2 weeks. PBS was used as it was isotonic to animal cells and prevented denaturation of proteins. At specific intervals, they were removed from PBS, washed in deionized water and freeze-dried. The weight of sample before immersing in PBS was Wi and final weight of sample after freeze-drying was W_t. The percentage of degradation was calculated by following equation. Triplicates of samples were done and the average was plotted.

$$\text{percentage of degradation}(\%) = 100 \times (W_i - W_t)/W_i$$

Dissolved Oxygen Measurements. Dissolved oxygen (DO) measurements were carried out using Hach luminescent dissolved oxygen electrode (LDO 101−01). It worked on the basic principle of dynamic luminescence quenching. Luminophores were materials which fluoresce when excited by light of a specific wavelength. When these materials encounter oxygen, their fluorescence was quenched. The dynamic lifetime of luminophore was measured and the result was used to compute DO. Z_F particles were suspended in deionized water at concentrations of 0.24, 0.48, 2.4, and 4.8% (w/v), respectively, and continuously stirred at 37 °C. A bottle containing deionized water was taken as the control. The LDO probe was immersed in sample and DO was recorded. Triplicates of samples were analyzed and the average was plotted.

Cell Viability Studies. Cytotoxicity of HA/gelatin/Z_F and HA/gelatin (control) scaffolds were determined using MTS assay. MTS is a standard colorimetric assay for measuring the activity of mitochondrial enzymes that reduce MTS [3-(4,5-dimethylthiazol-2-yl)-5-(3-carboxy methoxy phenyl)-2-(4-sulfophenyl)-2H-tetrazolium], into purple colored formazan, whose absorbance can be read at a wavelength of 490−500 nm.[41] The samples were cut into pieces of equal weights and UV sterilized overnight. NIH 3T3 fibroblasts were cultured in DMEM medium. The cells were seeded onto 24 well plates at a density of 5×10^4 cells/mL and incubated at 37 °C for 48h. After the incubation period, MTS solution was added to each well and further incubated at 37 °C for another 4h. The solution in each well was then well-mixed and transferred to 96 well plates, and its absorbance was measured at 495 nm using Microplate reader (Spectromax 180). The data were plotted with mean ± SD and percentage of cell viability was determined.

Wound Healing Experiment. Eight male Sprague−Dawley rats (200−250g) were purchased from Genetic Improvement and Farm Technologies Sdn Bhd Malaysia. The rats were acclimatized to laboratory conditions for 1 week, before inducing wound. All experiments were carried out following the ethical guidelines of OECD Environment, Health and Safety, Malaysia. On the day of experiment (day 0), rats were anesthetized with a mixture of ketamine (90 mg/kg) and xylazin (10 mg/kg). The dorsal area of rats was shaved and cleaned with 70% ethanol. Partial thickness wound was induced on the operative area by adding 6 mL of hot water at 80 °C, through a concentric ring for 1 min, in nine repetitive cycles. Once the wound was induced, they were dressed with GH(2.4%) scaffold using standard gauze and 3 M adhesive tape. Group 1 constituted rats whose wounds

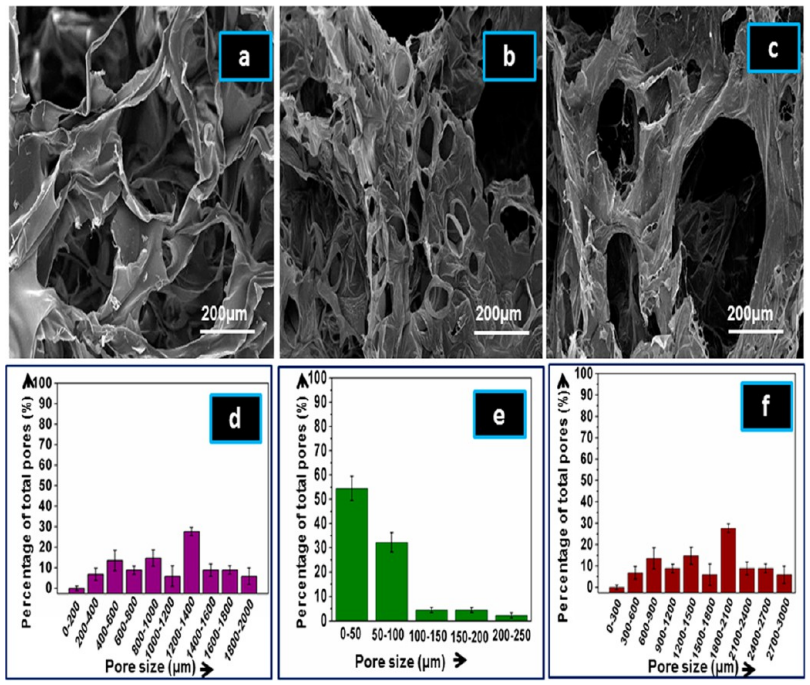

Figure 2. SEM images of (a) GH(0%), (b) GH(2.4%), and (c) GH(4.8%), which displayed well interconnected pores for GH(2.4%). Pore size distribution of (d) GH(0%), (e) GH(2.4%), and (f) GH(4.8%), showing that GH(2.4%) was the optimized scaffold with pore size in the range of 10−250 μm.

were not treated and group 2 consisted of rats which were covered with scaffolds. During the experiment, the rats were housed in individual cages wiped with 70% alcohol swab and maintained at 25 °C, in a 12 h light/dark cycle, They were supplied with food and drinking water, during post wounding. Every day the wound area was dressed with scaffold material and morphology of wound was captured using an Optical Steady Shot digital camera (Sony DSC-W730, Malaysia). The wound area was plotted on a tracing sheet and the radius was measured using a digital micrometer. The percentage of wound area was determined by preceding equation and then tabulated. Data was expressed as mean ± SD and statistical analysis was carried out using Student's t test. A value of $p < 0.05$ was considered statistically significant.

$$\text{percentage of wound area closure}(\%) = 100 \times (A_0 - A)/A_0$$

where A_0 is the initial wound area calculated on day 0 and A is the wound area on day t.

Histological Assessment of Open Wound. On day 8, the rats were sacrificed and skin of the wound area was excised, immersed in isotonic saline solution and stored at −20 °C in a deep freezer until use. The skin was fixed onto glass slides using Jung tissue freezing medium (Leica, Germany) and cut into thin sections using a cryostat (Leica CM1950, Germany). Around 8 sections were prepared for each sample which were stained by hematoxylin and eosin in Autostainer XL (Leica, Germany) and visualized using compound microscope (Leica DF2500, Germany), fitted with a camera to capture representative digital images.

RESULTS AND DISCUSSION

In the current study, gelatin/HA/faujasite composite scaffolds were fabricated by lyophilization technique. A probable mechanism for the formation of composite scaffold was demonstrated in Figure 1. Gelatin polypeptide chains adopted coil configuration when heated at 60 °C and attained positive charge at pH ∼3.7, below its isoelectric point (pH ∼4.5).[42] HA was found to swell badly in water and adopted negative charge. As HA was added by syringe addition to gelatin suspension, the latter binds to former. To this polymer solution, sonicated faujasite suspension was added, such that negatively charged faujasite particles bind to the positively charged segments of gelatin. Once faujasites were dispersed within the polymer matrix, the suspension was then instantly cross-linked by formaldehyde. During formaldehyde cross-linking, lysine and arginine residues present in gelatin were converted to their respective methylols, which further linked to form lysine-arginine cross-links. Thus, gelatin underwent coil to helix transformation.[43] The cross-linked viscous solution was poured into petriplates and then frozen at −20 °C. During freeze-drying, ice crystals grew and were phase-separated from polymeric solution and the frozen solvent was removed by sublimation under vacuum, resulting in the formation of pores.

Morphology Analysis Using SEM. The surface morphologies of GH(0%), GH(2.4%), and GH(4.8%), were analyzed using SEM. GH(2.4%) and GH(4.8%) were chosen to visualize the morphology of scaffolds impregnated with low and high concentration of Z_F. Figure 2 depicted that pores were continuous and well interconnected in case of GH(2.4%) but poorly interconnected in case of GH(0%) and GH(4.8%). The pore size was in the range of 50−2000 μm for GH(0%), 10−250 μm for GH(2.4%), and 100−3000 μm for GH(4.8%). The average pore size of GH(0%) was 551.2 ± 9.7 μm, that of GH(2.4%) was 59.8 ± 6.5 μm, and that for GH(4.8%) was 1950 ± 2.3 μm. The highest number of pores were found in the range of 400−600 μm in case of GH(0%), 5−50 μm for GH(2.4%), and 1800−2100 μm for GH(4.8%).

Figure 3a showed that Z_F particles have octahedral morphology and were found in the size range of 0.5−1 μm. Images c and d in Figure 3 revealed that Z_F particles were uniformly dispersed (represented by arrows) throughout GH(2.4%), whereas agglomeration (represented by encircled regions) was observed in the case of composite scaffolds with higher concentration of Z_F, GH(4.8%). GH(0%) contained bigger pores, whereas the sizes of pores were greatly reduced by

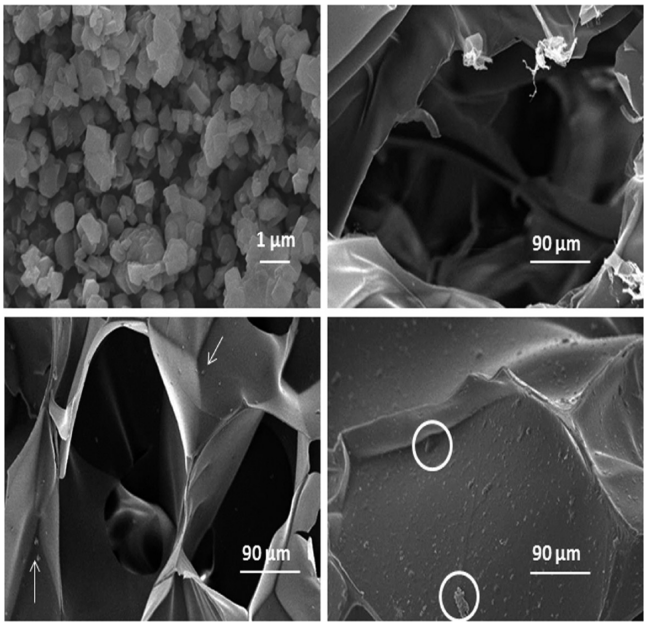

Figure 3. SEM images of (a) Z_F particles, (b) GH (0%) without Z_F, (c) uniform dispersion of Z_F within the matrix of GH(2.4%), and (d) agglomeration of Z_F in GH(4.8%).

the incorporation of 2.4% (w/v) of Z_F in the polymer matrix. This may be due to the good interaction of negatively charged Z_F with the positively charged amino acids of gelatin. However, GH(4.8%) contained biggest pores among the prepared scaffolds because with increase in concentration of faujasites, the viscosity of composite solution increased which offered high resistance to the ice crystal growth during lyophilization that resulted in the formation of micro cracks and eventually gave rise to bigger pores. At high concentration of Z_F, the interaction between Z_F−Z_F became dominant compared to polymer−Z_F, resulting in agglomeration of Z_F particles and hence poor reinforcement of Z_F within the polymer matrix, which can be another reason for the formation of large pores. From previous investigations, the pore size was found to be 100−200 μm for gelatin/HA scaffold;[27] 75−150 μm for gelatin/HA/chondroitin sulfate;[29] 350 μm for gelatin containing artificial skin[44] and 189 μm for gelatin/HA cross-linked by carbodiimide.[45] Earlier reports stated that pores of 100−300 μm allowed cell colonization and vascularization, leading to tissue penetration into the scaffolds.[46] Compared with the literature, the obtained pore size distribution for GH(2.4%) was ideal for dermal tissue engineering.

In the EDX spectra of GH(0%), the peaks corresponding to carbon, oxygen and nitrogen were assigned to biopolymers, namely, gelatin and HA. The EDX spectra of GH(2.4%) and GH(4.8%) contained peaks corresponding to sodium, aluminum, and silicon besides the peaks mentioned above (Figure 4),

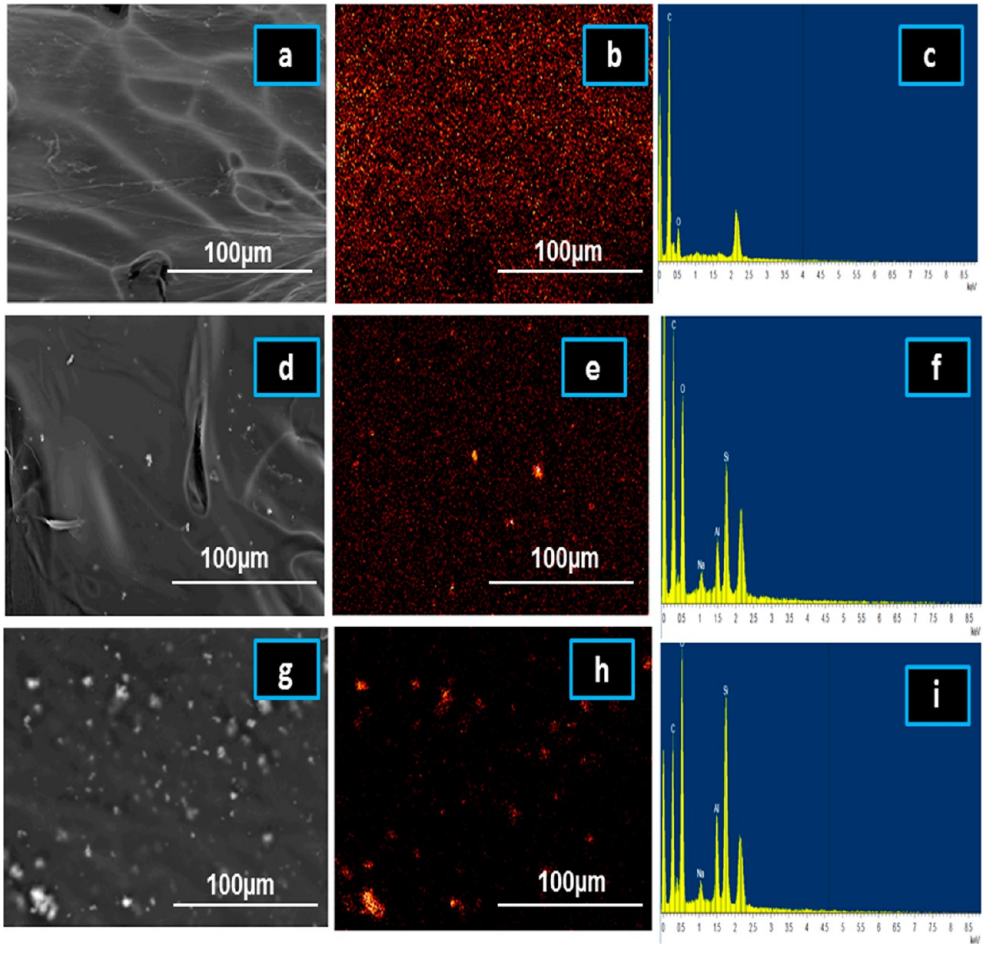

Figure 4. SEM images, EDX silicon mapping, and EDX spectra of (a−c) GH(0%), (d−f) GH(2.4%), and (g−i) GH(4.8%). Yellow dots in the silicon mapping showed the presence of Z_F within the scaffold matrix.

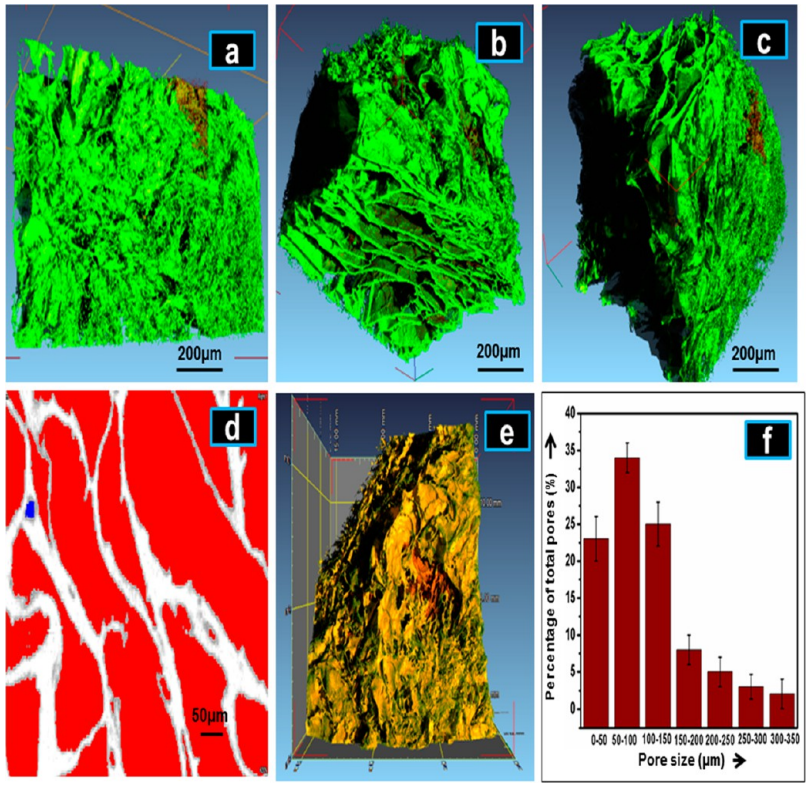

Figure 5. Micro-CT images of (a) top, (b) bottom, (c) side,and (d) cross-sectional views of GH(2.4%), which exhibited a porosity of 90% estimated by (e) defect volume analysis. (f) Pore size distribution of GH(2.4%) was found to be in the range of 10−350 μm.

which were attributed by Z_F particles dispersed in the polymer matrix. The peak corresponding to oxygen became more prominent in case of composite scaffolds due to aluminosilicates present in Z_F. The intensity of peaks contributed by Z_F got amplified with the rise in concentration of Z_F in the composite scaffold. Literature has provided evidence that Si/Al ratio for Y-type zeolites like faujasites is 3, and we obtained similar result for the composites and Z_F, showing that Z_F particles have maintained their composition even though they were embedded within the polymer matrix.[47] From the silicon mapping, it was obvious that Z_F particles were uniformly dispersed in GH(2.4%), whereas agglomeration was observed in the case of GH(4.8%).

Micro-CT Analysis. Micro-CT was employed to obtain 3D images, porosity and pore size distribution of the optimized scaffold, GH(2.4%). Compared to SEM, it can be used to investigate the internal morphology of the porous scaffold. The pore size was found in the range of 10−350 μm and the highest number of pores were found in the range of 50−100 μm. The obtained pore size value was greater than that attained by SEM analysis because micro-CT measured the pore diameters in terms of pixels present in the pore.[48] Moreover, SEM can only evaluate the pore size at the external surface, whereas micro-CT can analyze internal pores as well. In spite of such differences in technique, the pore size of GH(2.4%) identified by SEM and micro-CT analyzer was significantly smaller than GH(0%) and GH(4.8%). Figure 5 displayed the top, bottom and side views of GH(2.4%), which showed that pores were well-interconnected and distributed throughout the scaffold, in agreement with SEM.

Porosity is a vital factor that increases surface area for cells to adhere which is an essential criteria for tissue engineering scaffolds.[49] From the defect volume analysis, the sample volume was 104.98 mm^3 and defect volume was 1011.7 mm^3. The porosity was estimated to be 90.6%, which was in agreement with earlier report that scaffolds need minimum porosity of 90% for allowing cell growth and proliferation.[50]

Contact Angle Measurements. The surface wettability of control and composite scaffolds were evaluated in detail. Table 1

Table 1. List of Contact Angle and Surface Energy of GH(0%), GH(0.24%), GH(0.48%), GH(2.4%), and GH(4.8%)

samples	contact angle with water (deg)	contact angle with formamide (deg)	contact angle with tricresyl phosphate (deg)	surface energy (mJ/m^2)
GH(0%)	92 ± 1.71	59 ± 2.05	44 ± 1.84	54
GH(0.24%)	97 ± 1.02	63 ± 1.77	48 ± 2.5	52.4
GH(0.48%)	108 ± 2.19	77 ± 1.05	59 ± 1.73	48.3
GH(2.4%)	117 ± 3.44	81 ± 2.81	68 ± 1.45	45.5
GH(4.8%)	77 ± 2.03	42 ± 2.06	34 ± 2.017	58.9

showed that hydrophobicity of composite scaffold increased on the addition of Z_F till GH(2.4%) and then decreased drastically for GH(4.8%). Both HA and gelatin were water-soluble but the control scaffold, GH(0%), exhibited hydrophobic nature as they were cross-linked by formaldehyde. Keeping the concentration of polymer and cross-linker constant, we tried to evaluate the effect of increase in concentration of faujasite on surface energy of composite. The contact angle of GH(0%) was 92 ± 1.71° for water, 59 ± 2.05° for formamide and 44 ± 1.84° for tricresyl phosphate. GH(2.4%) exhibited contact angles of 117 ± 3.44° for water, 81 ± 2.81° for formamide and 68 ± 1.45° for tricresyl phosphate (Figure 8D). Because gelatin was the major component in the composite, it can be assumed that negatively charged Z_F might have interacted with positively charged amino acids of gelatin, resulting in reorientation of hydrophobic amino acids chains which were exposed to the surface.[51] This might be a

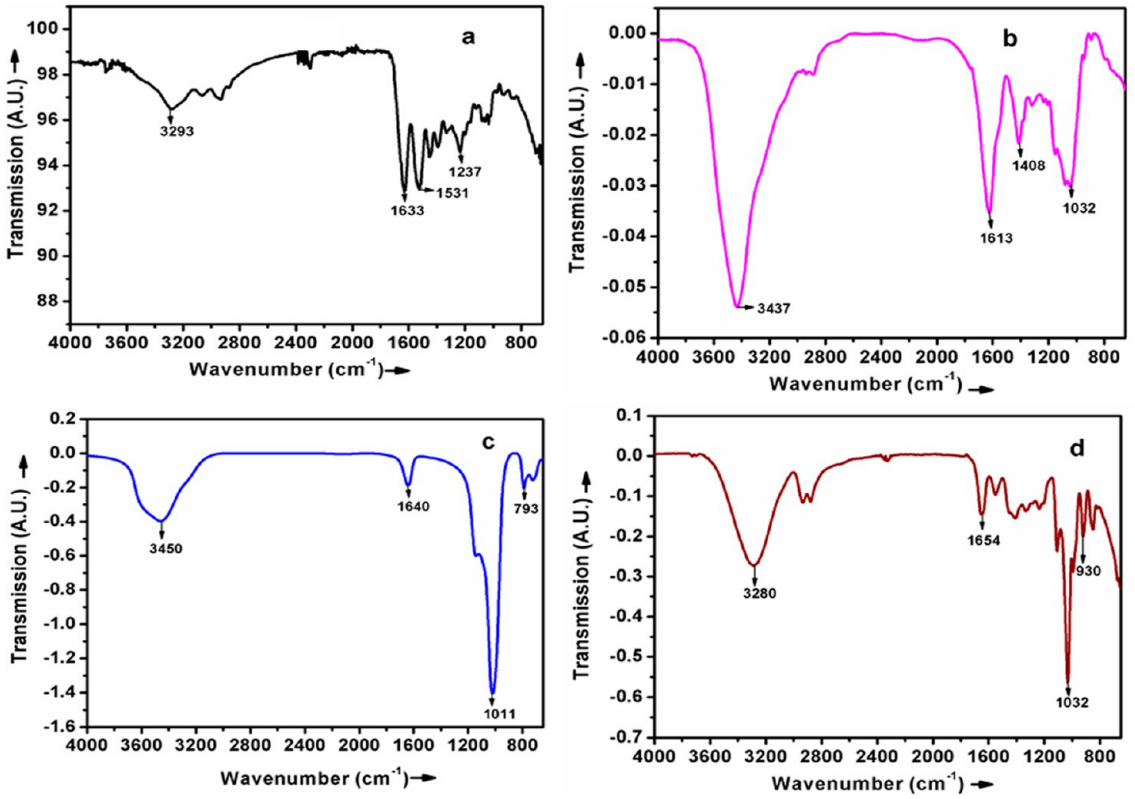

Figure 6. FTIR spectra of (a) gelatin, (b) HA, (c) Z_F, (d) gelatin/HA/Z_F hybrid scaffold showed evidence for cross-linking by formaldehyde and possible interactions between polymer and Z_F within the composite.

possible reason for the increase in hydrophobicity with addition of Z_F in the polymer matrix. In the case of GH(4.8%), more Z_F particles were dispersed on the surface as evident from SEM image (Figure 2f). Z_F particles have good affinity to water and can increase surface energy.[52] Another explanation for the increase in the hydrophobicity is given by Cassie−Wenzel approach, which states that if air is trapped within the pores of the material, it can probably increase the contact angle.[53] Surface hydrophobicity was a key factor to evaluate cell response as it affects the rate of cell spreading and differentiation.[54] A highly hydrophilic surface may not yield high level of cellular attachment.[55] A moderately hydrophobic surface of GH(2.4%) with small pores between 5 and 50 μm and a minimum porosity of 90% were ideal for cellular attachment and dermal fibroblast infiltration and growth.

FTIR and XRD Analysis. The possible interactions between gelatin, HA, Z_F and the mode of cross-linking were studied using FTIR (Figure 6). The typical FTIR peaks of gelatin were amide A peak at 3293 cm^{-1} due to −NH stretching vibration, amide I band at 1633 cm^{-1} assigned to −CO stretching vibration, amide II band at 1531 cm^{-1} corresponding to −NH bend coupled with −CH stretch, and amide III band at 1237 cm^{-1} due to −NH bend.[56] The distinctive FTIR peaks of HA were observed at 1613 cm^{-1} due to −CO stretching vibration, 1455 cm^{-1} corresponding to ester band for −CO stretch, and 1048 cm^{-1} representing −C−O−C stretching vibration.[45] The characteristic FTIR peaks of Z_F were found in the range of 1250−900 cm^{-1} because of asymmetrical Si −O −Si or Al −O −Al stretching.[57] The entire representative peaks of gelatin, HA and Z_F were found in the FTIR spectra of the composite scaffold with minor shifts. The peaks at 1025 cm^{-1} was shifted to 930 cm^{-1} due to electrostatic interaction between negatively charged faujasite and positively charged amino acids of gelatin.[58] During formaldehyde cross-linking, lysine and arginine residues present in gelatin got converted to their respective methylols which further linked to form cross-linked gelatin. As a result, amide I band of gelatin was shifted from 1633 to 1654 cm^{-1} and amide II band was shifted from 1531 to 1554 cm^{-1}, because of the presence of a greater number of weak hydrogen bonds in aqueous environment, in the case of composite scaffold. Also, the peak at 3280 cm^{-1} was broadened because of hydrogen bonding interaction within the composite.

Figure 7 represented the XRD spectra of GH(0%), which proved that it was amorphous. The diffractogram denoted the highly crystalline peak of Z_F. 2θ of faujasite was observed at 4.4° due to (111) plane. Other characteristic diffraction peaks of Z_F were 11.09, 14°, 16.87,19.07, and 22.01° attributed by (311),

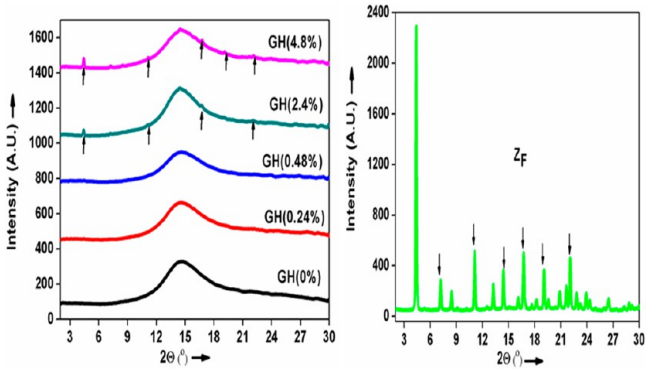

Figure 7. XRD spectra of GH(0%), GH(0.24%), GH(0.48%), GH(2.4%), GH(4.8%), and Z_F confirmed that embedded Z_F maintained their crystallinity within the composite.

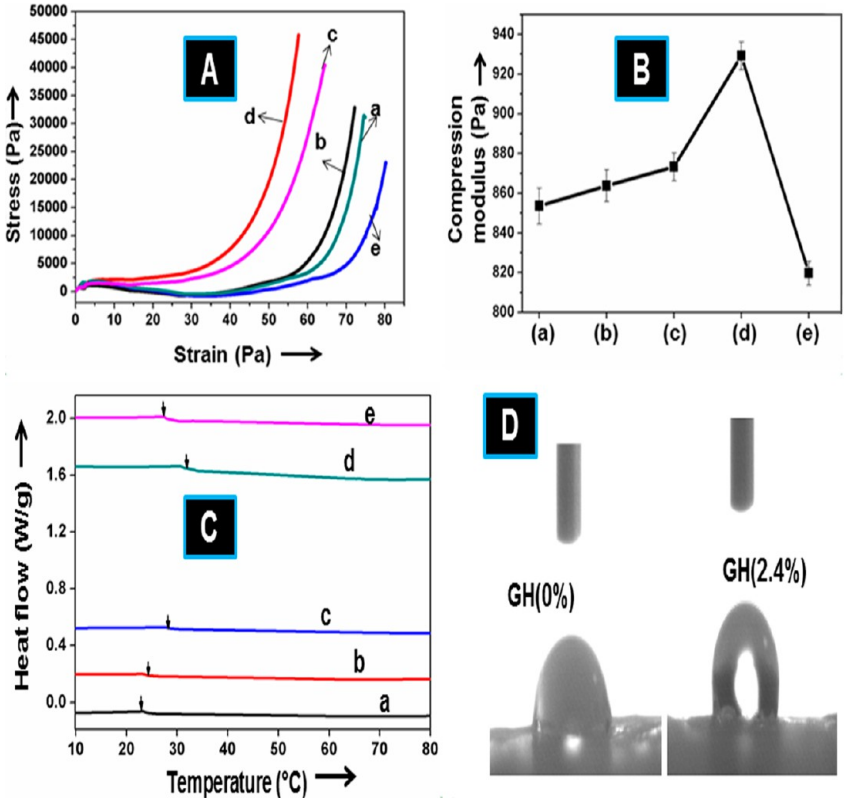

Figure 8. (A) Stress/strain curves, (B) change in compression modulus, and (C) DSC analysis of (a) GH(0%), (b) GH(0.24%), (c) GH(0.48%), (d) GH(2.4%), and (e) GH(4.8%), confirmed that GH(2.4%) has got the highest thermal and mechanical stability. (D) Images of water drops on (a) GH(0%) and (b) GH(2.4%), after 30 s, showed that GH(2.4%) had a moderately hydrophobic surface suitable for growth of dermal fibroblasts.

(400), (422), (440), and (533), respectively.[59] These peaks were found in the XRD spectra of the composite scaffolds whose intensity increased with increase in the concentration of Z_F. The results confirmed that Z_F particles maintained their crystallinity in the polymer matrix inspite of the interactions between polymer and Z_F, as proved from FTIR analysis.

Mechanical and Thermal Properties. From DMA analysis, compression modulus increased monotonously with increase in concentration of Z_F till GH(2.4%) and decreased drastically on further addition of Z_F. The compression modulus of GH(0%) was 853 ± 9 Pa, whereas that of GH(2.4%) was 929 ± 7 Pa (Figure 8A, B). This was attributed due to good polymer−filler interaction with increasing fraction of Z_F till GH(2.4%). These Z_F particles transferred the applied load from the polymer chains to nearby Z_F particles, thereby avoided the formation of microcracks in the system.[60] H(4.8%) demonstrated a compression modulus of 819 ± 6 Pa. The possible reason for the drop in mechanical strength was that ice crystals grew by pushing aside the polymer chains into the ice grain boundaries, during lyophilization. At low concentration of Z_F, the viscosity of the composite solution was less and hence it offered small resistance to the growth of ice front. At higher viscosity, the growth of ice crystal would be retarded, resulting in fractal growth and secondary crystallization of water, leading to poor interconnectivity of pores and increase in pore size and hence lower mechanical strength.[60]

DSC outlined glass transition as a change in the heat capacity when the polymer matrix goes from glassy state to rubbery state and it appears as a step transition in the DSC spectra.[61] In a material with low glass transition temperature (T_g), polymer chains can easily move and less heat was required to commence wiggling and transition from the rigid glassy state into a soft rubbery state. Whereas huge amount of heat was required for the transition to take place in case of polymers with high T_g.[62] GH(0%) underwent segmental mobility at low temperature (~22 ± 0.9 °C) as it contained more free volume (Figure 8C). With increase in free volume, T_g would drop. In GH(2.4%), the uniform distribution of Z_F within the polymer matrix, hindered the segmental motions and increased the relaxation time. As a result, more heat was required for transition and hence the T_g value increased (~31 ± 0.05 °C). On the other hand, GH(4.8%) had a comparatively lower T_g because agglomerated Z_F particles limited the close packing of polymer chains and increased the free volume. Thus, DSC results were in concordance with DMA analysis.

Stability of Scaffolds in Water and Buffer. Water uptake ability was an essential property of scaffolds that enabled easy diffusion of nutrients to the cells and better absorption of culture medium. It can be controlled by changing the concentration of fillers or monitoring the cross-linking density. It can be affected by several factors like porosity, size of pores, crystallinity and free volume.[63] The water uptake ability of gelatin/HA control scaffold and gelatin/HA/Z_F composite scaffold was demonstrated in Figure 9A. Z_F incorporated composite scaffold showed lower swelling percentage compared to control scaffold. This may be due to good interaction between Z_F and the polymers, which resulted in improved mechanical integrity. The effective reinforcement shielded the polymer backbone, thereby avoiding penetration of water molecules. On the other hand, GH(0%) demonstrated uncontrolled swelling as it contained large free volume for the water molecules to accumulate and migrate. On day 2, the percentage of water uptake was 77 ± 2% for GH(0%)

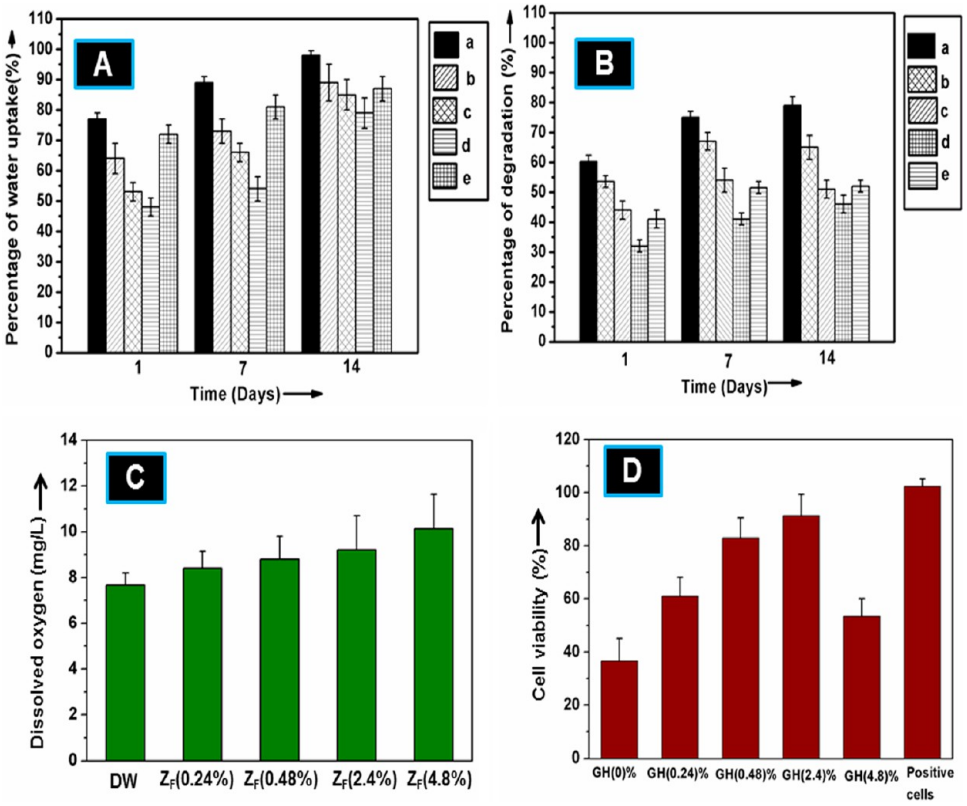

Figure 9. (A) Water uptake analysis and (B) In vitro degradation profile of (a) GH(0%), (b) GH(0.24%), (c) GH(0.48%), (d) GH(2.4%), (e) GH(4.8%) demonstrated that swelling and degradation can be highly controlled by incorporation of Z_F. (C) Dissolved oxygen concentrations in deionized water at 37 °C in the presence of different weight percentages of faujasites, confirmed the ability of Z_F to increase oxygen supply to cells. (D) Cell viability of GH(0%), GH(0.24%), GH(0.48%), GH(2.4%), GH(4.8%), and control fibroblast cells stating that GH(2.4%) exhibited the highest cytocompatibility.

while it was greatly reduced to 48 ± 3% for GH(2.4%). On day 14, the percentage of water uptake was 98 ± 1.5% and 79 ± 5.3% for GH(0%) and GH(2.4%) respectively. With the increase in concentration of Z_F, the rate of water uptake was found to decrease till GH(2.4%). On further increasing the concentration of Z_F, swelling was found to increase due to bigger pores present in the scaffold formed as a result of poor interaction of polymers and Z_F along with agglomeration of Z_F particles. The results proved that swelling of scaffolds can be controlled by varying the concentration of Z_F.

The in vitro degradation profile of gelatin/HA control scaffold and gelatin/HA/Z_F composite scaffold was shown in Figure 9B. On seventh day, GH(0%) underwent 60 ± 2% degradation, whereas GH(2.4%) showed 32 ± 2% degradation. On the fourteenth day, the percentage of degradation of GH(0%) and GH(2.4%) were 79 ± 3% and 46 ± 2% respectively. The possible reason for decrease in the degradation rate was good interaction between Z_F and polymer matrix. The degradation rate decreased with increase in concentration of Z_F till GH(2.4%). However, GH(4.8%) showed an increase in degradation rate due to poor reinforcing effect of Z_F in the polymer matrix and inefficient cross-linking. We conducted EDX analysis of degraded GH(2.4%) scaffold and verified that that Z_F still existed in the matrix (refer to the Supporting Information). A fast degrading material cannot support cell proliferation, whereas a slow degrading material can result in stress shielding which was threatening for the tissue growth.[64] Thus, controlled swelling and degradation property was imperative to ensure that the pore size would not be excessively large or small which in turn could negate cellular infiltration.

Dissolved Oxygen (DO) Measurements. We tried to explore whether faujasite particles were capable of increasing DO concentration in water and thereby meet the oxygen supply demands for the growth of skin fibroblasts. The LDO probe consisted of a measuring light emitting diode (LED) that emitted blue light along with a photo detector. When LED emitted blue light, the sensing filament produced red photons that were captured by detector. The intensity and time delay were measured. When more oxygen molecules were present in the medium, the intensity and duration of red radiation were lowered and these changes were used to calculate DO. It was found that with the increase in concentration of Z_F particles, the DO was found to increase (Figure 9C). This can be explained by the presence of more oxygen molecules in the medium which were involved in luminescence quenching. Structurally, faujasite consisted of pores with a diameter of 7 Å, which was sufficient to accommodate oxygen molecules with a size of 1.21 Å.[65] When Z_F particles were dispersed in water, oxygen trapped within the pores diffused into water as they were held by weak Vander Waals forces and thereby increased the level of DO in water. The experiment revealed the ability of Z_F to supply oxygen to needy dermal fibroblasts.

Cell Viability Studies. Cytocompatibility of gelatin/HA and gelatin/HA/Z_F composite scaffolds were assessed on NIH3T3 cell line using MTS assay. Positive cells constituted NIH 3T3 fibroblast cells which were not exposed to samples. Among the tested samples, GH(2.4%) showed the highest cell viability (91 ±

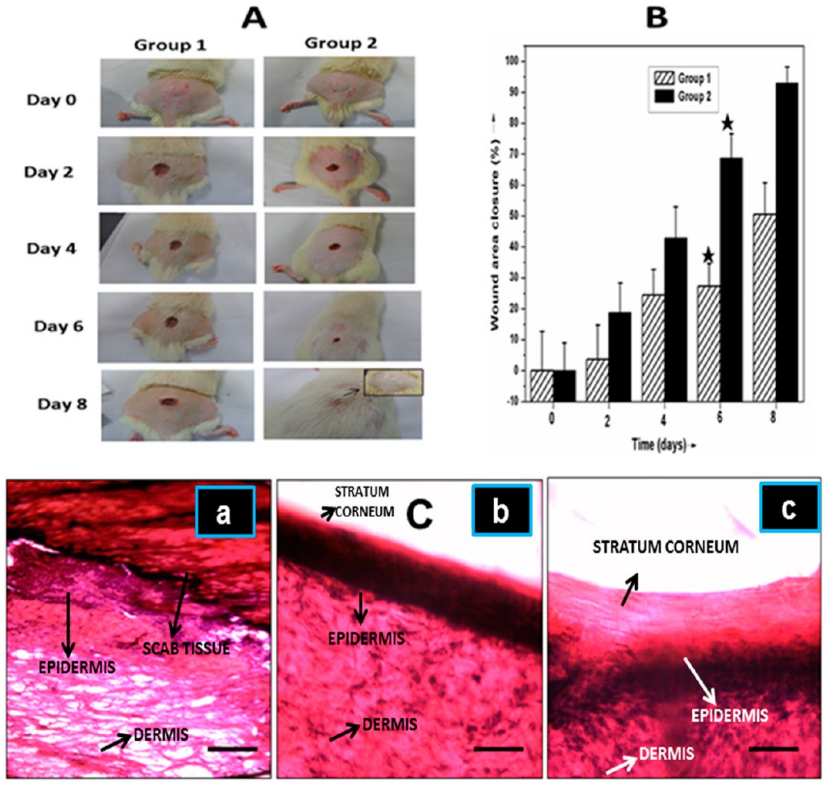

Figure 10. (A) Macroscopic pictures of partial thickness wound at specific time points (0, 2, 4, 6, and 8 days) and (B) analysis of wound area closure (%) for 8 days in the case of group 1 (untreated) and group 2 (treated with GH(2.4%)) rats. All data reported as mean ± SD,* $p < 0.05$. (C) Histological examinations comparing the morphology of epidermis and part of dermis in case of (a) group 1, (b) group 2, and (c) normal rats on day 8.

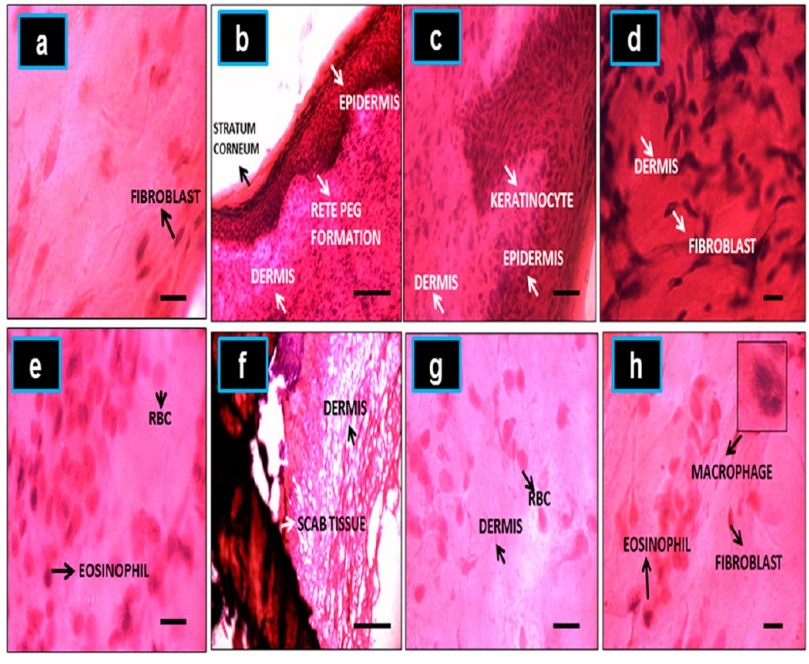

Figure 11. Histological sections of group 2 rats treated with GH(2.4%) and group 1 rats (untreated) at lower and higher magnification. The images showed (a) presence of fibroblasts (at 100×) on day 3, (b) rete peg formation (at 20×), (c) densely packed keratinocytes in epidermis (at 40×), and (d) fibroblast in the dermis (at 100×), in the case of group 2 rats on day 8. Group 1 rats showed (e) increase in inflammatory cells (at 100×) on day 3, (f) white empty spaces in the dermis due to poor collagen deposition (at 20×), (g) poor infiltration of fibroblasts (at 100×), and (h) presence of eosinophils and macrophages along with fibroblasts (at 100×), on day 8, revealing the chances of persistent inflammation.

8%) after 48h (Figure 9D). The uniform dispersion of Z_F in the polymer matrix rendered it to have high porosity, mechanical strength and reduced swelling and degradation. The ideal pore size of GH(2.4%) in the range of 10−250 μm with porosity of ∼90.6% facilitated the growth of fibroblasts. Also, Z_F (2.4%) was found to increase the oxygen supply and this can be another

dx.doi.org/10.1021/am403436y | ACS Appl. Mater. Interfaces 2013, 5, 11194−11206

possible reason for high cell viability. GH(0%) and GH(4.8%) exhibited low cell viability (36 ± 8.4%) as they had large pores (proved from SEM analysis) which were not suitable for fibroblast growth. They showed uncontrolled swelling and the leachate products increased the viscosity of DMEM medium, making them unfit for fibroblasts to grow. Compared to positive cells, there was no significant reduction in cell viability for GH(2.4%), suggesting it to be biocompatible.

In vivo Studies. From the experiments, GH(2.4%) was the optimized scaffold with good cell viability, highest mechanical strength, controlled swelling, and degradation. As a result, the wound healing ability of GH(2.4%) was further studied in this section. Group 2 constituted Sprague–Dawley rats treated with GH(2.4%) and group 1 included the control rats whose wounds were left open. As observed in Figure 10A, single round partial thickness wound was created on the dorsal area of each rat in which the entire epidermis and a part of dermis was destroyed. On day 0, wounded skin adopted white eschar with hyperemic zone at the wound border. Soon, white eschar was transformed into a state of full hyperemia where there was an increase in blood flow to the injured area.[16] The wound size of group 2 rats was significantly smaller when compared to group 1 rats, as observed on 2, 4, 6, and 8 days. They exhibited faster reduction in wound size and higher re-epithelization propensity than group 1 (Figure 10B). The hair was completely grown on eighth day, for rats treated with GH(2.4%). On the other hand, control rats took 31 days for full re-epithelization.

Histological Analysis. From Figure 10C, the thickness of epidermis can be compared in case of group1, group 2 and normal rats. Complete re-epithelization or regrowth of new cutaneous tissue at the wound site was observed in case of group 2 rats on eighth day. The stratum corneum was found to be thinner compared to normal rats as they have attained only 90% wound healing. In case of group 1 rats, epidermis and dermis were poorly organized beneath a thick scab tissue, on eighth day. The white empty spaces in the dermis revealed poor collagen deposition, whereas collagen was uniformly deposited throughout the extracellular matrix of group 2 rats.[66]

On third day, the level of inflammation was intensified in case of group 1 rats, whereas it was greatly reduced in case of group 2 rats. There were more red blood cells (RBC) because of breaching of blood vessels and inflammatory cells at the wound site (Figure 11a).

For rats treated with GH(2.4%) scaffold, the epithelial and dermal tissues were revived from the base of wound bed and cell migration occurred from the border of the wound to central portion of the wound, on the eigth day. Epithelial tongue was observed at the edge of wound margin because of the migration of keratinocytes to the injured area in order to cover the wound (Figure 11c). Prominent rete pegs were found which confirmed the advanced stages of wound healing (Figure 11b). Fibroblasts, the principal cells of remodelling phase, were evenly distributed in the dermis (Figure 11d), and were involved in collagen synthesis.[67] Mild inflammation was observed in case of group 1 rats on the eighth day. The presence of eosinophils and macrophages along with fibroblasts confirmed the possibility of inflammation (Figure 11h). Macrophages phagocytized bacteria and generated several growth factors that promoted fibroblast proliferation.[68] Thus, GH(2.4%) were promising substrates for stimulating skin regeneration in rat models.

CONCLUSION

Gelatin/HA/faujasite scaffolds were successfully fabricated using lyophilization technique. The composite membrane with 2.4% (w/w) faujasites exhibited high porosity and low surface energy that were favorable for the growth of dermal fibroblasts. The presence of crystalline faujasites in the composite scaffold was confirmed by EDX and XRD spectra and their interaction with polymers were studied using FTIR. Because of the effective reinforcement of faujasites, it showed high mechanical strength, glass transition temperature and controlled swelling and degradation. It demonstrated high cell viability and the in vivo results on Sprague–Dawley rats proved that the composite scaffold brought about 90% healing of partial thickness wound in eight days. All these results suggested the use of gelatin/HA/faujasite porous scaffolds as excellent wound dressing materials.

ASSOCIATED CONTENT

Supporting Information

SEM and EDX plot confirmed the presence of faujasite in degraded GH(2.4%) scaffold. This material is available free of charge via the Internet at http://pubs.acs.org

AUTHOR INFORMATION

Corresponding Author

*E-mail: neethuninan85@yahoo.co.in. Tel.: +33751464109. Fax. +33 (0)2 97 87 45 19.

Author Contributions

The manuscript was written through contributions of all authors. All authors have given approval to the final version of the manuscript.

Notes

The authors declare no competing financial interest.

ACKNOWLEDGMENTS

We deeply acknowledge the financial support provided by Brittany region, The European Union (FEDER) and the French Ministry for research for conducting the studies.

ABBREVIATIONS

Z_F, faujasite
HA, hyaluronic acid
GH(0%), control scaffold without Z_F
GH(0.24%), composite scaffold with 0.24% Z_F
GH(0.48%), composite scaffold with 0.48% Z_F
GH(2.4%), composite scaffold with 2.4% Z_F
GH(4.8%), composite scaffold with 4.8% Z_F
Z_F(0.24%), 0.24% of faujasites in water
Z_F(0.48%), 0.48% of faujasites in water
Z_F(2.4%), 2.4% of faujasites in wate
Z_F(4.8%), 4.8% of faujasites in water
DW, distilled water
SEM, scanning electron microscope
EDX, energy-dispersive X-ray spectroscopy
Micro-CT, micro computed tomography
FTIR, Fourier transform infrared spectroscopy
XRD, X-ray diffraction
DSC, differential scanning calorimetry
2D, two-dimensional
V_1, defect volume
V_2, volume of scaffold
T_g, glass transition temperature
PBS, phosphate buffered saline

W_1, weight of sample before immersing in water
W_2, weight of sample after immersing in water
W_i, weight of sample before immersing in PBS
W_t, final weight of sample after freeze-drying
DMEM, Dulbecco's Modified Eagle Medium
MTS, 3-(4,5-dimethyl thiazole-2-yl)-5-(3-carboxy methoxy phenyl)-2-(4-sulfo phenyl)-2H- tetrazolim
A_0, initial wound area calculated on day 0
A, wound area on day t
SD, standard deviation

REFERENCES

(1) Choi, J. S.; Leong, K. W.; Yoo, H. S. *Biomaterials* **2008**, *29*, 587−596.
(2) Kim, B.-S.; Park, I.-K.; Hoshiba, T.; Jiang, H.-L.; Choi, Y.-J.; Akaike, T.; Cho, C.-S. *Prog. Polym. Sci.* **2011**, *36*, 238−268.
(3) Ziv-Polat, O.; Topaz, M.; Brosh, T.; Margel, S. *Biomaterials* **2010**, *31*, 741−747.
(4) Caiado, F.; Carvalho, T.; Silva, F.; Castro, C.; Clode, N.; Dye, J. F.; Dias, S. *Biomaterials* **2011**, *32*, 7096−7105.
(5) Gong, C.; Wu, Q.; Wang, Y.; Zhang, D.; Luo, F.; Zhao, X.; Wei, Y.; Qian, Z. *Biomaterials* **2013**, *34*, 6377−6387.
(6) Xi, Y.; Dong, H.; Sun, K.; Liu, H.; Liu, R.; Qin, Y.; Hu, Z.; Zhao, Y.; Nie, F.; Wang, S. *ACS Appl. Mater. Interfaces* **2013**, *5*, 4821−4826.
(7) Choi, J. K.; Jang, J.-H.; Jang, W.-H.; Kim, J.; Bae, I.-H.; Bae, J.; Park, Y.-H.; Kim, B. J.; Lim, K.-M.; Park, J. W. *Biomaterials* **2012**, *33*, 8579−8590.
(8) Kumar, P. T. S.; Abhilash, S.; Manzoor, K.; Nair, S. V.; Tamura, H.; Jayakumar, R. *Carbohydr. Polym.* **2010**, *80*, 761−767.
(9) Jayakumar, R.; Prabaharan, M.; Sudheesh Kumar, P. T.; Nair, S. V.; Tamura, H. *Biotechnol. Adv.* **2011**, *29*, 322−337.
(10) Thu, H.-E.; Zulfakar, M. H.; Ng, S.-F. *Int. J. Pharm.* **2012**, *434*, 375−383.
(11) Vasconcelos, A.; Gomes, A. C.; Cavaco-Paulo, A. *Acta Biomater.* **2012**, *8*, 3049−3060.
(12) Ulubayram, K.; Cakar, A. N.; Korkusuz, P.; Ertan, C.; Hasirci, N. *Biomaterials* **2001**, *22*, 1345−1356.
(13) de Almeida, E. B.; Cordeiro Cardoso, J.; Karla de Lima, A.; de Oliveira, N. L.; de Pontes-Filho, N. T.; Oliveira Lima, S.; Leal Souza, I. C.; de Albuquerque-Júnior, R. L. C. *J. Ethnopharmacol.* **2013**, *147*, 419−425.
(14) Xie, Y.; Upton, Z.; Richards, S.; Rizzi, S. C.; Leavesley, D. I. *J. Controlled Release* **2011**, *153*, 225−232.
(15) Zhang, L.; Li, K.; Xiao, W.; Zheng, L.; Xiao, Y.; Fan, H.; Zhang, X. *Carbohydr. Polym.* **2011**, *84*, 118−125.
(16) Ramli, N. A.; Wong, T. W. *Int. J. Pharm.* **2011**, *403*, 73−82.
(17) Li, Y.; Chen, F.; Nie, J.; Yang, D. *Carbohydr. Polym.* **2012**, *90*, 1445−1451.
(18) Song, B.; Wu, C.; Chang, J. *Acta Biomater.* **2012**, *8*, 1901−1907.
(19) Unnithan, A. R.; Barakat, N. A. M.; Tirupathi Pichiah, P. B.; Gnanasekaran, G.; Nirmala, R.; Cha, Y.-S.; Jung, C.-H.; El-Newehy, M.; Kim, H. Y. *Carbohydr. Polym.* **2012**, *90*, 1786−1793.
(20) Aquino, R. P.; Auriemma, G.; Mencherini, T.; Russo, P.; Porta, A.; Adami, R.; Liparoti, S.; Porta, G. D.; Reverchon, E.; Del Gaudio, P. *Int. J. Pharm.* **2013**, *440*, 188−194.
(21) Darroudi, M.; Ahmad, M. B.; Abdullah, A. H.; Ibrahim, N. A. *Int. J. Nanomedicine* **2011**, *6*, 569−574.
(22) Tronci, G.; Neffe, A. T.; Pierce, B. F.; Lendlein, A. *J. Mater. Chem.* **2010**, *20*, 8875−8884.
(23) Saraogi, G. K.; Gupta, P.; Gupta, U. D.; Jain, N. K.; Agrawal, G. P. *Int. J. Pharm.* **2010**, *385*, 143−149.
(24) Kim, H.-W.; Kim, H.-E.; Salih, V. *Biomaterials* **2005**, *26*, 5221−5230.
(25) Matsuda, T.; Saito, Y.; Shoda, K. *Biomacromolecules* **2007**, *8*, 2345−2349.
(26) Oh, E. J.; Park, K.; Kim, K. S.; Kim, J.; Yang, J.-A.; Kong, J.-H.; Lee, M. Y.; Hoffman, A. S.; Hahn, S. K. *J. Controlled Release* **2010**, *141*, 2−12.
(27) Collins, M. N.; Birkinshaw, C. *Carbohydr. Polym.* **2013**, *92*, 1262−1279.
(28) Camci-Unal, G.; Cuttica, D.; Annabi, N.; Demarchi, D.; Khademhosseini, A. *Biomacromolecules* **2013**, *14*, 1085−1092.
(29) Wang, T.-W.; Sun, J.-S.; Wu, H.-C.; Tsuang, Y.-H.; Wang, W.-H.; Lin, F.-H. *Biomaterials* **2006**, *27*, 5689−5697.
(30) Kumar, P.; Sung, C.-Y.; Muraza, O.; Cococcioni, M.; Al Hashimi, S.; McCormick, A.; Tsapatsis, M. *Microporous Mesoporous Mater.* **2011**, *146*, 127−133.
(31) Bresinska, I.; Balkus, K. J., Jr. *J. Phys. Chem. C* **1994**, *98*, 12989−12994.
(32) Ferreira, L.; Fonseca, A. M.; Botelho, G.; Aguiar, C. A.; Neves, I. C. *Microporous Mesoporous Mater.* **2012**, *160*, 126−132.
(33) Amorim, R.; Vilaça, N.; Martinho, O.; Reis, R. M.; Sardo, M.; Rocha, J.; Fonseca, A. M.; Baltazar, F.; Neves, I. C. *J. Phys. Chem. C* **2012**, *116*, 25642−25650.
(34) Seifu, D. G.; Isimjan, T. T.; Mequanint, K. *Acta Biomater.* **2011**, *7*, 3670−3678.
(35) Morsli, A.; Bengueddach, A.; Di Renzo, F.; Quignard, F. In *Zeolites and Related Materials: Trends and Challenges*; Gédéon, A., Massiani, P., Babonneau, F., Eds.; Studies in Surface Science and CatalysisElsevier: Amsterdam, 2008; Vol.*174*, p 1143.
(36) Yu, L.; Gong, J.; Zeng, C.; Zhang, L. *Mater. Sci. Eng., C* **2013**, *33*, 3652−3660.
(37) Cohen, B.; Sanchez, F.; Douhal, A. *J. Am. Chem. Soc.* **2010**, *132*, 5507−5514.
(38) Calero, S.; Dubbeldam, D.; Krishna, R.; Smit, B.; Vlugt, T. J. H.; Denayer, J. F. M.; Martens, J. A.; Maesen, T. L. M. *J. Am. Chem. Soc.* **2004**, *126*, 11377−11386.
(39) Lopes, A. C.; Silva, M. P.; Gonçalves, R.; Pereira, M. F. R.; Botelho, G.; Fonseca, A. M.; Lanceros-Mendez, S.; Neves, I. C. *J. Phys. Chem.C* **2010**, *114*, 14446−14452.
(40) Zhuang, Y. X.; Hansen, O. *Langmuir* **2009**, *25*, 5437−5441.
(41) Vavříková, E.; Mandíková, J.; Trejtnar, F.; Horváti, K.; Bösze, S.; Stolaříková, J.; Vinšová, J. *Carbohydr. Polym.* **2011**, *83*, 1901−1907.
(42) Zandi, M.; Mirzadeh, H.; Mayer, C. *Eur. Polym. J.* **2007**, *43*, 1480−1486.
(43) Chen, X.; Jia, Y.; Feng, L.; Sun, S.; An, L. *Polymer* **2009**, *50*, 2181−2189.
(44) Lee, S. B.; Kim, Y. H.; Chong, M. S.; Hong, S. H.; Lee, Y. M. *Biomaterials* **2005**, *26*, 1961−1968.
(45) Zhang, F.; He, C.; Cao, L.; Feng, W.; Wang, H.; Mo, X.; Wang, J. *Int. J. Biol. Macromol.* **2011**, *48*, 474−481.
(46) Katoh, K.; Tanabe, T.; Yamauchi, K. *Biomaterials* **2004**, *25*, 4255−4262.
(47) Ninan, N.; Grohens, Y.; Elain, A.; Kalarikkal, N.; Thomas, S. *Eur. Polym. J.* **2013**, *49*, 2433−2445.
(48) Dubruel, P.; Unger, R.; Van Vlierberghe, S.; Cnudde, V.; Jacobs, P. J. S.; Schacht, E.; Kirkpatrick, C. J. *Biomacromolecules* **2007**, *8*, 338−344.
(49) Lee, B. L.-P.; Tang, Z.; Wang, A.; Huang, F.; Yan, Z.; Wang, D.; Chu, J. S.; Dixit, N.; Yang, L.; Li, S. *Acta Biomater.* **2013**, *9*, 7264−7275.
(50) Ninan, N.; Muthiah, M.; Park, I.-K.; Elain, A.; Thomas, S.; Grohens, Y. *Carbohydr. Polym.* **2013**, *98*, 877−885.
(51) Farris, S.; Introzzi, L.; Biagioni, P.; Holz, T.; Schiraldi, A.; Piergiovanni, L. *Langmuir* **2011**, *27*, 7563−7574.
(52) Perego, C.; Bagatin, R.; Tagliabue, M.; Vignola, R. *Microporous Mesoporous Mater.* **2013**, *166*, 37−49.
(53) Wang, X.; Ding, B.; Yu, J.; Wang, M. *Nano Today* **2011**, *6*, 510−530.
(54) Kato, D.; Takeuchi, M.; Sakurai, T.; Furukawa, S.-i.; Mizokami, H.; Sakata, M.; Hirayama, C.; Kunitake, M. *Biomaterials* **2003**, *24*, 4253−4264.
(55) Okano, T.; Yamada, N.; Okuhara, M.; Sakai, H.; Sakurai, Y. *Biomaterials* **1995**, *16*, 297−303.
(56) Chen, Y.-C.; Su, W.-Y.; Yang, S.-H.; Gefen, A.; Lin, F.-H. *Acta Biomater.* **2013**, *9*, 5181−5193.
(57) Frolich, K.; Bulanek, R.; Frydova, E. *Microporous Mesoporous Mater.* **2013**, *171*, 185−195.

(58) Zou, T.; Percival, S. S.; Cheng, Q.; Li, Z.; Rowe, C. A.; Gu, L. *Eur. J. Pharm. Biopharm.* **2012**, *82*, 36−42.
(59) Tiaw, K. S.; Teoh, S. H.; Chen, R.; Hong, M. H. *Biomacromolecules* **2007**, *8*, 807−816.
(60) Chen, H.-B.; Chiou, B.-S.; Wang, Y.-Z.; Schiraldi, D. A. *ACS Appl. Mater. Interfaces* **2013**, *5*, 1715−1721.
(61) Ford, J. L.; Mann, T. E. *Adv. Drug Delivery Rev.* **2012**, *64*, 422−430.
(62) Naffakh, M.; Díez-Pascual, A. M.; Marco, C.; Ellis, G. J.; Gómez-Fatou, M. A. *Prog. Polym. Sci.* **2013**, *38*, 1163−1231.
(63) Monfregola, L.; Bugatti, V.; Amodeo, P.; De Luca, S.; Vittoria, V. *Biomacromolecules* **2011**, *12*, 2311−2318.
(64) Zhong, S. P.; Zhang, Y. Z.; Lim, C. T. *Wiley Interdiscip. Rev. Nanomed. Nanobiotechnol.* **2010**, *2*, 510−525.
(65) Coutant, M. A.; Payra, P.; Dutta, P. K. *Microporous Mesoporous Mater.* **2003**, *60*, 79−90.
(66) Sudheesh Kumar, P. T.; Lakshmanan, V.-K.; Anilkumar, T. V.; Ramya, C.; Reshmi, P.; Unnikrishnan, A. G.; Nair, S. V.; Jayakumar, R. *ACS Appl. Mater. Interfaces* **2012**, *4*, 2618−2629.
(67) Wang, P.; Zhou, S.; Xu, L.; Lu, Y.; Yuan, X.; Zhang, H.; Li, R.; Fang, J.; Liu, P. *J. Ethnopharmacol.* **2013**, *145*, 152−161.
(68) Smallwood, H. S.; López-Ferrer, D.; Squier, T. C. *Biochemistry* **2011**, *50*, 9911−9922.